Journal of Non-Crystalline Solids: X 19 (2023) 100196

Contents lists available at ScienceDirect

Journal of Non-Crystalline Solids: X

journal homepage: www.sciencedirect.com/journal/journal-of-non-crystalline-solids-x

Ultrafast third-order nonlinear optical response of charge coupled gold nanoparticle-$Ge_{24}Se_{76}$ heterostructure

Vinod Kumar [a], Rituraj Sharma [a], Abhishek Bhatt [a], I. Csarnovics [b], Petr Nemec [c], H. Jain [d], K.V. Adarsh [a,*]

[a] Department of Physics, Indian Institute of Science Education and Research Bhopal, 462066, India
[b] Department of Experimental Physics, Institute of Physics, Faculty of Science and Technology, University of Debrecen, 4032 Debrecen, Hungary
[c] Department of Graphic Arts and Photophysics, Faculty of Chemical Technology, University of Pardubice, 53210 Pardubice, Czech Republic
[d] Department of Materials Science and Engineering, Lehigh University, Bethlehem, Pennsylvania 18015, USA

ARTICLE INFO

Keywords:
$AuNP/Ge_{24}Se_{76}$ heterostructure
Nonlinear optical response
Two-photon absorption
Nonlinear refractive index
Saturable absorption

ABSTRACT

The donor-acceptor interaction of a charge-coupled heterostructure encompassing a metal and an amorphous semiconductor subjected to a laser field has many potential applications in the realm of nonlinear optics. In this work, we fabricate an electron donor gold nanoparticle (AuNP) and acceptor amorphous $Ge_{24}Se_{76}$ heterostructure on a quartz substrate using a sequential thermal evaporation technique. In this charge coupled heterostructure, we demonstrate the ultrafast third-order nonlinear absorptive and refractive response, and their sign reversal compared to pristine $Ge_{24}Se_{76}$. Enhanced optical nonlinearity in these heterostructures of varying plasmonic wavelengths is due to charge transfer, verified by the Raman spectroscopy. Further, the ultrafast transient absorption measurements support the thesis of charge transfer in the $AuNP/Ge_{24}Se_{76}$ heterostructure. These findings open up exciting opportunities for developing novel device technologies with far-reaching applications in nonlinear optics.

1. Introduction

Metal-semiconductor heterostructures have attracted significant attention owing to their unique optoelectronic properties and potential applications [1–3]. These heterostructures offer tunable and versatile platforms for various optoelectronic devices, including ultrafast optical limiters [4,5] and passive mode-locking saturable absorbers for ultrashort laser pulses [6,7]. The interaction between donor and acceptor components in these heterostructures, typically involving metals and semiconductors, has been a subject of extensive investigation due to the creation of a space-charge region, enabling the design of multifunctional properties not achievable in individual materials [8–10]. Over the years, many metal-semiconductor heterostructures have been realized, such as metal-core/semiconductor-shell structures and non-epitaxially coupled metal-semiconductor hybrids (both organic and inorganic), demonstrating tailored optical properties for applications in optical limiters, photovoltaics, solar cells, and photodetectors [5,11–13]. The charge-transfer interaction in these heterostructures has proven to be a powerful mechanism for modifying their chemical and optoelectronic properties [14,15]. Notably, recent studies have reported exceptional enhancements in the third-order nonlinear optical response through efficient charge transfer from metal shells to semiconductor cores triggered by selective excitation at the plasmonic wavelength [16]. Similarly, charge-coupled systems like single-wall carbon nanotube-VSe_2 have exhibited remarkable enhancements in the nonlinear optical response across a broad spectral range (400–900 nm) [17]. Large enhancements in third-order nonlinear optical responses have also been observed in heterostructures such as $MoSe_2$/graphene oxide [8], gold nanoparticles (AuNP)/reduced graphene oxide [5], gold-cadmium sulfide [18], and gold-cadmium telluride [19] systems. Given these advancements, it becomes crucial to investigate the impact of charge transfer on the ultrafast third-order nonlinear optical response in the $AuNP/Ge_{24}Se_{76}$ heterostructure, particularly in the local field environment of the surface plasmon resonance of the metal nanoparticles. Understanding the intricate dynamics and optoelectronic behavior in this heterostructure will provide valuable insights for harnessing its potential in nonlinear optics and pave the way for future applications.

To address this challenge, we have used a thermal evaporation

* Corresponding author.
E-mail address: adarsh@iiserb.ac.in (K.V. Adarsh).

https://doi.org/10.1016/j.nocx.2023.100196
Received 1 June 2023; Received in revised form 14 July 2023; Accepted 5 August 2023
Available online 7 August 2023

process to synthesize a charge-coupled AuNP/$Ge_{24}Se_{76}$ heterostructure with various plasmonic wavelengths. By optimizing the plasmonic wavelength to coincide with the optical bandgap of $Ge_{24}Se_{76}$, we investigated the charge transfer between AuNP and $Ge_{24}Se_{76}$. This article presents our findings on ultrafast third-order nonlinear absorptive and refractive response in the charge-coupled AuNP/$Ge_{24}Se_{76}$ heterostructure using *Z*-scan measurements in the strong coupling regime facilitated through charge transfer. Remarkably, we have observed a sign reversal in the ultrafast nonlinear optical response of the heterostructure compared to pristine $Ge_{24}Se_{76}$. While $Ge_{24}Se_{76}$ exhibits weak two-photon absorption (TPA) and self-focusing (positive nonlinearity), the strongly coupled heterostructure demonstrates saturable absorption (SA) and self-defocusing (negative nonlinearity). Moreover, we observe a significant enhancement in the magnitude of the saturation intensity and nonlinear refractive index of AuNP/$Ge_{24}Se_{76}$ at various surface plasmon resonance wavelengths. For instance, the heterostructures exhibit a large saturation intensity of 98 ± 9 GW/cm^2 and a four-fold enhancement in the nonlinear refractive index, which has an opposite sign compared to $Ge_{24}Se_{76}$.

2. Experimental details

2.1. Raman spectroscopy

The Raman spectra were acquired using a Horiba LabRAM high-resolution spectrometer equipped with a 632.5 nm He—Ne laser as the excitation source. To prevent sample damage, the laser intensity at the sample surface was maintained at a low level (< 1 mW).

2.2. Z-scan measurement

For the Z-scan measurements, we employed a Ti: Sapphire Regenerative Amplifier System. The excitation source consisted of 120 fs pulses with an energy equivalent to 0.68 times the bandgap energy (E_g) of $Ge_{24}Se_{76}$. The femtosecond laser pulse was focused onto the sample using a plano-convex lens with a focal length of 30 cm. The sample position was controlled along the *Z*-axis using a motorized translation stage. In our experimental setup, the Rayleigh length (Z_0) was 1.8 mm, and the beam waist (W_0) was approximately 50 μm.

2.3. Ultrafast transient absorption measurements

In the ultrafast transient absorption measurements, an 800 nm laser beam with 120 fs pulses, 1 kHz repetition rate was employed. To generate the pump pulse, the initial laser beam was directed through an optical parametric amplifier (TOPAS), resulting in a 545 nm pump pulse with a fluence of 500 μJ/cm^2. The second pulse, serving as the probe pulse, was time-delayed using a computer-controlled translational stage and then focused onto a CaF_2 crystal plate generating white light spanning from 400 to 1000 nm. During the experiment, the pump and probe pulse were brought into spatial alignment on sample, and absorbance change of probe pulse was then determined as $\Delta A = -(\log [\frac{I_{ex}}{I_0}])$, where I_{ex} represented the transmitted intensity of the probe beam after a delay time of τ caused by pump pulse excitation, and I_0 represented the transmitted intensity in the ground state. Further the acquired traces were chirp-corrected using a previously reported technique [20].

3. Results and discussion

We fabricated a strongly coupled AuNP/$Ge_{24}Se_{76}$ heterostructure using a thermal evaporation technique [21–23]. Initially, a 15 nm thick gold layer was deposited onto a quartz substrate, which was then transformed into Au nanoparticles (AuNP) via Ostwald ripening by heating the film at various temperatures ranging from 350 to 550 °C [22–24]. This process resulted in different nanoparticle sizes with corresponding plasmonic wavelengths. For example, nanoparticles of sizes 60, 80, and 100 nm exhibited plasmon wavelengths of 545, 580, and 620 nm, respectively (Fig. 1(a)). The size and morphology of the AuNP were characterized using an atomic force microscope (AFM), and more details can be found elsewhere [21]. Subsequently, a 450 nm thick $Ge_{24}Se_{76}$ film was thermally evaporated over the AuNP to form the strongly coupled AuNP/$Ge_{24}Se_{76}$ heterostructure. To investigate the interaction between the AuNP and the pristine $Ge_{24}Se_{76}$ domains within the heterostructures, we performed conventional ultraviolet-visible dual-beam spectroscopy and measured the absorption spectra of the samples.

Fig. 1(a) displays the optical absorption spectrum of AuNP with a size of 60 nm, revealing a plasmon band centered at a wavelength of 545 nm. Notably, as the particle size increases to 80 and 100 nm, the plasmon wavelength shifts to longer wavelengths of 580 and 620 nm, respectively. Fig. 1(b) shows the optical absorption spectra of AuNP/$Ge_{24}Se_{76}$ heterostructure and pristine $Ge_{24}Se_{76}$. Both spectra exhibit a characteristic interference pattern, with the $Ge_{24}Se_{76}$ layer demonstrating lower absorbance levels compared to the AuNP/$Ge_{24}Se_{76}$ heterostructure, indicating the effect of metallic nanoparticles on the optical properties. Furthermore, the optical absorption spectrum of the heterostructure suggests a superposition of signals from the individual components; however, the overall signal has exhibited a redshift equated to pure $Ge_{24}Se_{76}$, signifying charge transfer and strong coupling between the AuNP and $Ge_{24}Se_{76}$. Additionally, Fig. 1(c) presents the optical absorption spectra of the heterostructure corresponding to three different plasmon wavelengths. It can be observed that the plasmon resonance undergoes a shift consistent with the size-dependent trend of metallic permittivity and plasmon oscillations [25,26]. Henceforth, we will refer to the AuNP/$Ge_{24}Se_{76}$ heterostructures as HS-1 (plasmon wavelength 545 nm), HS-2 (580 nm), and HS-3 (620 nm). We performed a Tauc plot analysis on the optical absorption spectra of the AuNP/$Ge_{24}Se_{76}$ heterostructures (HS-2) and $Ge_{24}Se_{76}$, as shown in Fig. 1(d) to find the optical bandgap. Our calculations revealed optical bandgap of 2.18 ± 0.03 and 2.24 ± 0.02 eV for AuNP/$Ge_{24}Se_{76}$ (HS-2) heterostructure and $Ge_{24}Se_{76}$, respectively. Interestingly, we observed that this bandgap value is in proximity to the surface plasmon resonance band of the AuNP. Strikingly, we observed 60 meV redshift in HS-2 compared to pristine $Ge_{24}Se_{76}$. This finding suggests a potential correlation between the optical bandgap of $Ge_{24}Se_{76}$ and the surface plasmon resonance wavelength of AuNP, indicating an opportunity for optimal coupling between the two materials.

To gain further insights into the coupling between AuNP and $Ge_{24}Se_{76}$, we conducted Raman spectroscopy measurements on both pristine samples and heterostructures. The resulting Raman spectra are presented in Fig. 2(a). The Raman spectrum of $Ge_{24}Se_{76}$ exhibits three distinct vibrational modes, each associated with specific bonding configurations. These modes include a 194 cm^{-1} band attributed to corner-sharing vibrations of Ge—Se tetrahedra, a sideband around 210 cm^{-1} associated to edge-sharing tetrahedra, and a broad peak at 256 cm^{-1} originating from Se—Se bonds within the polymeric chain of Se atom [27–29]. The interaction between the constituents in the heterostructure leads to modifications in these band positions, resulting in both stiffening and softening effects [30].

Notably, the intensities of the Ge—Se and Se—Se Raman contributions experience a significant enhancement in the heterostructure, reaching magnitudes up to five times higher than those in the pristine $Ge_{24}Se_{76}$. This enhancement can be ascribed to surface-enhanced Raman scattering facilitated by the presence of AuNP [31]. The interaction of light with the surface plasmon oscillations near the AuNP surface enables surface-enhanced Raman scattering to occur [32,33]. In this context, it is worth considering that the strong coupling and charge transfer between the AuNP and $Ge_{24}Se_{76}$ contribute to the observed enhancement. It is likely that only the symmetric vibrational modes of the sample are selectively enhanced through the Franck–Condon contribution, while both symmetric and nonsymmetric vibrations can be

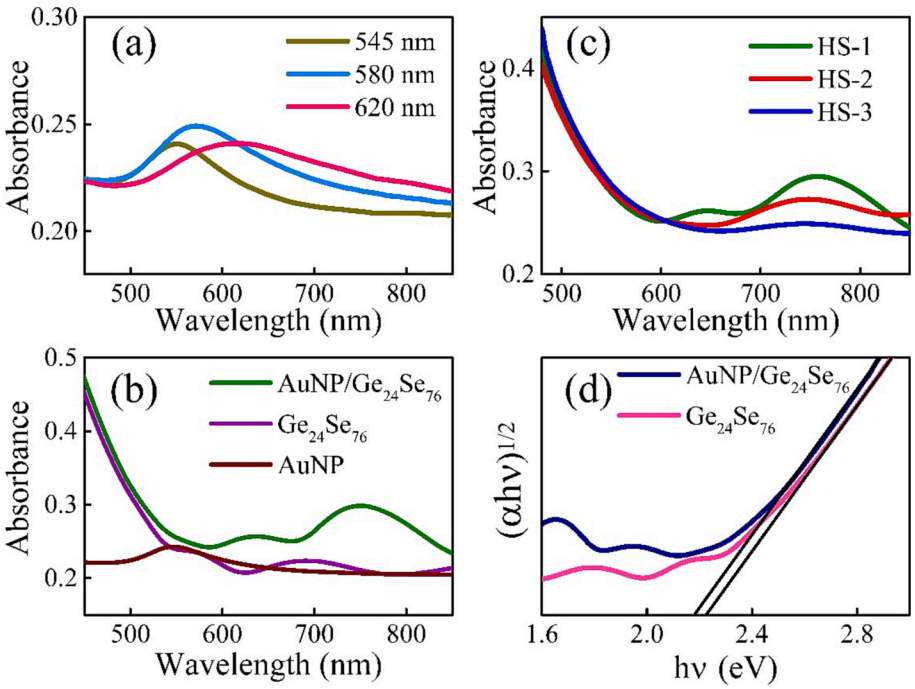

Fig. 1. (a) Optical absorption spectrum of AuNP revealing distinct plasmon bands at different wavelengths depending on the nanoparticle size. Specifically, nanoparticles with sizes of 60, 80, and 100 nm exhibit plasmon wavelengths of 545, 580, and 620 nm, respectively. (b) Optical absorption spectrum of AuNP/$Ge_{24}Se_{76}$ (HS-2) heterostructure, $Ge_{24}Se_{76}$ and AuNP. (c) Optical absorption spectrum of AuNP/$Ge_{24}Se_{76}$ heterostructures at various plasmon wavelengths. It can be observed that the overall spectrum of the heterostructure is redshifted compared to pristine $Ge_{24}Se_{76}$, indicating charge transfer and strong coupling between the AuNP and $Ge_{24}Se_{76}$ (d) The Tauc plot of AuNP/$Ge_{24}Se_{76}$ heterostructure (HS-2) and pristine $Ge_{24}Se_{76}$.

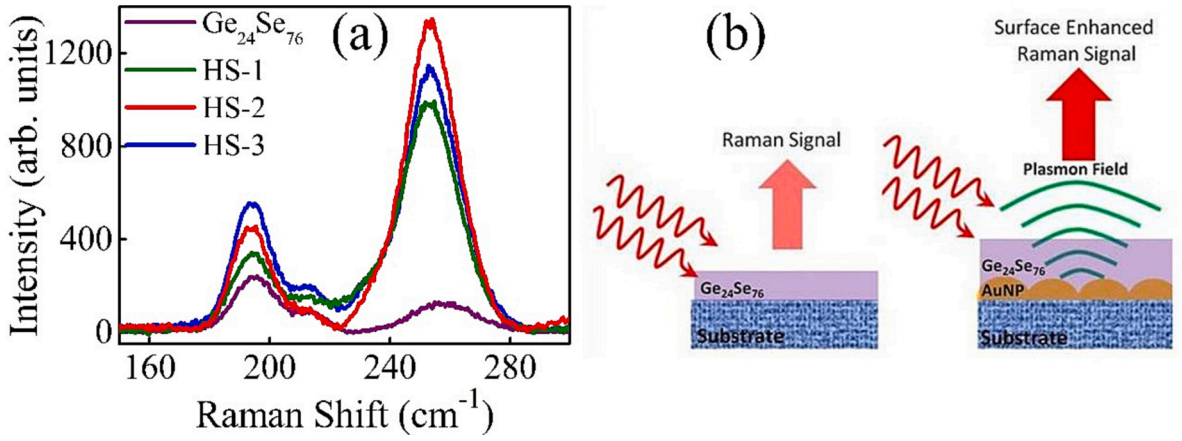

Fig. 2. (a) Raman spectrum of $Ge_{24}Se_{76}$ and AuNP/$Ge_{24}Se_{76}$ heterostructures. It is evident from the figure that the Raman spectrum of $Ge_{24}Se_{76}$ is significantly enhanced in the heterostructure. (b) Schematic showing the mechanism of plasmonic enhancement of Raman signals.

enhanced via the Herzberg–Teller effect [34]. Furthermore, we observe a similar enhancement of Raman signals across all heterostructures. Fig. 2(b) presents a schematic illustrating the process of plasmonic enhancement of the Raman signal. When the frequency of the exciting radiation resonates with the plasmon oscillation frequency, there is a significant increase in the dipolar electric field at the surface of the metal. This enhanced electric field substantially boosts the Raman signal of $Ge_{24}Se_{76}$ located on the surface of the AuNP [31,32].

To investigate the ultrafast third-order nonlinear optical response of the AuNP/$Ge_{24}Se_{76}$ heterostructures and pristine $Ge_{24}Se_{76}$, we conducted both open and closed aperture *Z*-scan measurements. These measurements enabled us to examine the overall transmittance as a function of the sample position at a particular intensity [8,17].

In Fig. 3(a), we present the open-aperture Z-scan results obtained at an on-axis peak intensity of 150 GW/cm^2 for the AuNP/$Ge_{24}Se_{76}$ heterostructures and pristine $Ge_{24}Se_{76}$, utilizing an 800 nm wavelength. In the case of pristine $Ge_{24}Se_{76}$, the Z-scan peak-shape trace demonstrates a reduction in transmission as it approaches the focal point, which is consistent with the two-photon absorption (TPA). It is important to note that this behavior is anticipated in $Ge_{24}Se_{76}$ due to the excitation at 800 nm falling within the two-photon excitation wavelength range. In stark contrast, the heterostructures exhibits saturable absorption (SA).

To quantify the observed nonlinear saturation intensity (I_s) and TPA coefficient (β), we employed the following differential equation [8,17] describing the nonlinear absorption,

$$\frac{dI}{dz} = -\alpha(I)I \tag{1}$$

where I represent the intensity and $\alpha(I)$ denotes the intensity-dependent absorption coefficient expressed as

$$\alpha(I) = \frac{\alpha_0}{I + \frac{I}{I_s}} + \beta I \tag{2}$$

where I_s and α_0 are, the saturation intensity and linear absorption coefficient, respectively. For a pulsed Gaussian beam, we can solve Eq. (1), and we can write the normalized transmittance T in the *Z*-scan experiment [8] as Eq. (3),

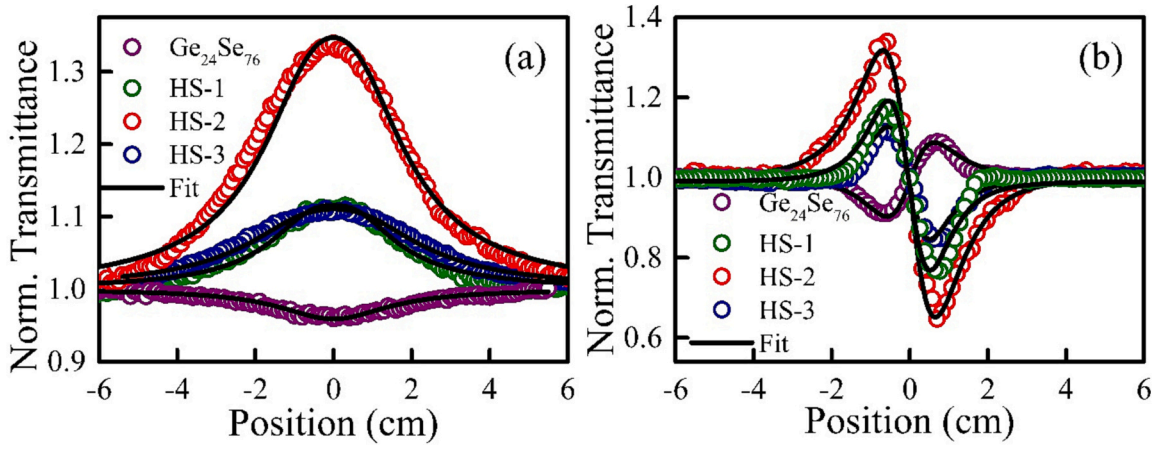

Fig. 3. Third-order nonlinear optical response of heterostructures and pristine $Ge_{24}Se_{76}$ at an on-axis peak intensity of 150 GW/cm^2 and 800 nm excitation. (a) Open aperture *Z*-scan traces (b) Closed aperture Z-scan traces (divided by open aperture Z-scan trace). Solid lines represent the numerical fits.

$$T = \left(\frac{1}{P_0\sqrt{\pi}}\right)\int_{-\infty}^{+\infty} ln\left(1 + P_0 e^{-t^2}\right)dt \tag{3}$$

Where P_0 is given by $P_0 = \left[\beta(1-R)I_0 L_{eff}\right] / \left[1 + (Z/Z_0)^2\right]$ R, Z_0, I_0, L and L_{eff} are the surface reflectively, Rayleigh length, peak intensity, length and effective length of the sample ($L_{eff} = (1 - e^{\alpha_0 L})/\alpha_0$). The parameters obtained from the optimal fit to the normalized transmittance data using Eq. (3) are presented in Table I. We can observe from Table I that the β value for pristine $Ge_{24}Se_{76}$ is determined to be β = (60 ± 5) × 10^{-2} cm/GW. Notably, the *Z*-scan trace of the AuNP did not exhibit any nonlinear behavior under the 800 nm excitation. However, the Z-scan peak-shape responses of the heterostructures displayed a remarkable increase in transmittance, indicating SA response. This behavior starkly contrasts the TPA observed in $Ge_{24}Se_{76}$ and the absence of nonlinearity in the AuNP. The saturation intensity (I_s) for the heterostructure (HS-2) is determined to be I_s = (98 ± 9) GW/cm^2 at the surface plasmon resonance wavelength of 580 nm, which is ~50 times larger than pristine $Ge_{24}Se_{76}$ in the femtosecond regime. This finding demonstrates the significant transition from TPA to SA in the heterostructure. Additionally, the calculated ground state absorption cross-section (σ_{GS}) and excited state cross-section (σ_{ES}) (shown in Table I) support the experimental evidence of the SA response of the samples [17]. According to the condition for observing SA, the σ_{GS} must be greater than the σ_{ES}, [8,17] and this condition is satisfied in all heterostructures. However, in the case of pristine $Ge_{24}Se_{76}$ σ_{GS} is less than the σ_{ES} resulting in TPA. We assume the larger value of σ_{GS} in heterostructure is due to charge transfer. Interestingly, Table I reveals no clear trend in the saturation intensity values concerning the plasmon wavelength.

After illustrating the nonlinear absorption using the open aperture *Z*-scan, we conducted a closed aperture Z-scan measurement to demonstrate the magnitude and sign of the nonlinear refractive index of the heterostructure and pristine $Ge_{24}Se_{76}$ in the femtosecond regime. We estimated the nonlinear refractive index (n_2) value by fitting the closed aperture *Z*-scan traces with the theoretical Eq. (4) [35],

$$T_N(y) = 1 + \frac{1}{\sqrt{2}}\frac{4\,y\,\varphi_0 - (y^2+3)p_0}{(y^2+1)(y^2+9)} + \frac{1}{\sqrt{3}}\frac{4\,\varphi_0{}^2(3y^2-5) + p_0{}^2(y^4+17y^2+40) - 8\varphi_0 p_0 y(y^2+9)}{(y^2+1)^2(y^2+9)(y^2+25)} \tag{4}$$

where T_N is the normalized transmittance, y = Z/Z_0 is the sample position, $p_0 = \beta I_0(1-R)L_{eff}$ is the phase shift, $\varphi_0 = 2\pi n_2 I_0(1-R)L_{eff}/\lambda$ is the on-axis phase shift with n_2. Fig. 3(b) showcases the closed aperture *Z*-scan traces for the heterostructures and $Ge_{24}Se_{76}$ at a moderate peak intensity of 150 GW/cm^2 and excitation wavelength of 800 nm. At this modest intensity, we observed a valley in the pre-focal position followed by a peak in the post-focal position, i.e. (valley-peak) indicating a positive refractive nonlinearity in pristine $Ge_{24}Se_{76}$. This behavior suggests a self-focusing nature of the material with an n_2 value of (1.5 ± 0.2) × 10^{-6} cm^2/GW. This positive refractive nonlinearity can be attributed to bound carriers generated due to nonresonant excitation. However, a surprising observation was made for the AuNP/$Ge_{24}Se_{76}$ heterostructures, where the Z-scan signature switched to a peak-valley structure. This indicates a negative refractive nonlinearity, leading to the self-defocusing nature of the material. The HS-2 exhibited an n_2 value of -(6.0 ± 0.5) × 10^{-6} which is ~50 times of $Ge_{24}Se_{76}$. The measured n_2 values are summarized in Table I, which indicates that the AuNP/$Ge_{24}Se_{76}$ heterostructure shows a higher n_2 compared to the pristine

Table I
Nonlinear optical parameters: TPA Coefficient (β), Saturation Intensity (I_s) and nonlinear refractive index (n_2), σ_{GS} and σ_{ES}.

Sample	β (10^{-2} cm/GW)	I_s (GW/cm^2)	σ_{GS} × 10^{-20} (cm^2)	σ_{ES} × 10^{-20} (cm^2)	n_2 (10^{-6} cm^2/GW)
$Ge_{24}Se_{76}$	60 ± 5	2.0 ± 0.4	1.5 ± 0.3	3.5 ± 0.4	1.5 ± 0.2
Au	–	–	–	–	–
HS-1	-(5.0 ± 0.4)	48 ± 4	4.8 ± 0.2	1.6 ± 0.2	-(2.7 ± 0.3)
HS-2	-(2.0 ± 0.3)	98 ± 9	8.6 ± 0.8	2.5 ± 0.5	-(6.0 ± 0.5)
HS-3	-(4.0 ± 0.5)	42 ± 3	4.5 ± 0.5	1.5 ± 0.2	-(2.5 ± 0.4)

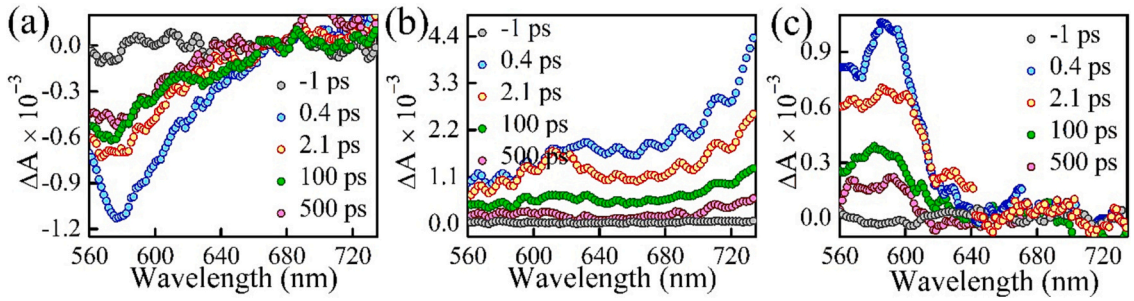

Fig. 4. Transient absorption spectrum of (a) AuNP (b) pristine $Ge_{24}Se_{76}$ and (c) HS-2 heterostructure at various probe delays.

$Ge_{24}Se_{76}$. Notably, the negative value of n_2 can be ascribed to the predominance of free carriers in the system [35]. This analysis allows us to quantitatively determine the nonlinear refractive properties of the samples and provides valuable insights into the interaction between the AuNP and $Ge_{24}Se_{76}$ in the heterostructure.

To gain a comprehensive understanding of the experimental findings pertaining to the charge transfer observed through third-order nonlinear optical measurements in the charge-coupled AuNP/$Ge_{24}Se_{76}$ heterostructures, we carried out femtosecond transient absorption (TA) measurements with the fluence of 500 μJ/cm^2. To illustrate these results, we present Fig. 4(a), which showcases the TA spectrum of AuNP at various probe delays. The spectrum indicates that the surface plasmon resonance peak aligns with the wavelength range demonstrating significant photobleaching. The observed bleach in the TA can be attributed to the broadening of the surface plasmon resonance caused by quadruple (non-dipolar) plasma oscillations induced by the pump pulse [36]. Fig. 4(b) illustrates the TA spectrum of $Ge_{24}Se_{76}$, encompassing the spectral range from the bandgap to the sub-bandgap regions.

The spectrum exhibits absorption maxima in the sub-bandgap region [37], providing compelling evidence for the self-trapped excitonic band [38,39]. Remarkably, the TA spectrum of HS-2 (Fig. 4(c)) exhibits a dramatic reduction in the TA signal within the sub-bandgap region. This observation provides compelling evidence for the strong coupling between self-trapped excitons and localized surface plasmons in the AuNP/$Ge_{24}Se_{76}$ heterostructures.

In order to deliver a comprehensive explanation for the observed quenching of TA in the heterostructures, we consider that the photoexcited electrons are effectively transferred from AuNP to $Ge_{24}Se_{76}$, which hinders the self-trapping of excitons and results in substantial reduction of photoinduced absorption in the below bandgap region of the $Ge_{24}Se_{76}$. This hypothesis is reinforced by empirical evidence, which demonstrates that the plasmon absorption signal (i.e., the AuNP photobleaching signal) is also quenched. Specifically, upon irradiation by the pump beam, the photoexcited electrons transfer from AuNP to $Ge_{24}Se_{76}$, resulting in the accumulation of a negative charge on the latter. Fig. 5(a-c) displays contour plots of TA spectra for the three heterostructures, HS-1, HS-2, and HS-3. Strikingly, it is evident from the figure that the magnitude of photoinduced absorption reduces significantly as the plasmonic wavelength reaches near the bandgap of pristine $Ge_{24}Se_{76}$.

Furthermore, Fig. 5(d) presents a plot of the photoinduced absorption maxima at 807 nm as a function of the plasmon wavelength. This plot highlights that the most effective exciton quenching occurs when the surface plasmon resonance reaches the bandgap. Thus, the TA quenching in AuNP/$Ge_{24}Se_{76}$ heterostructures can be precisely controlled by regulating the plasmonic wavelength, which is determined by the size of the AuNP. The plasmon wavelength dependence of transient absorption suggests that the size of the AuNP directly impacts the charge transfer.

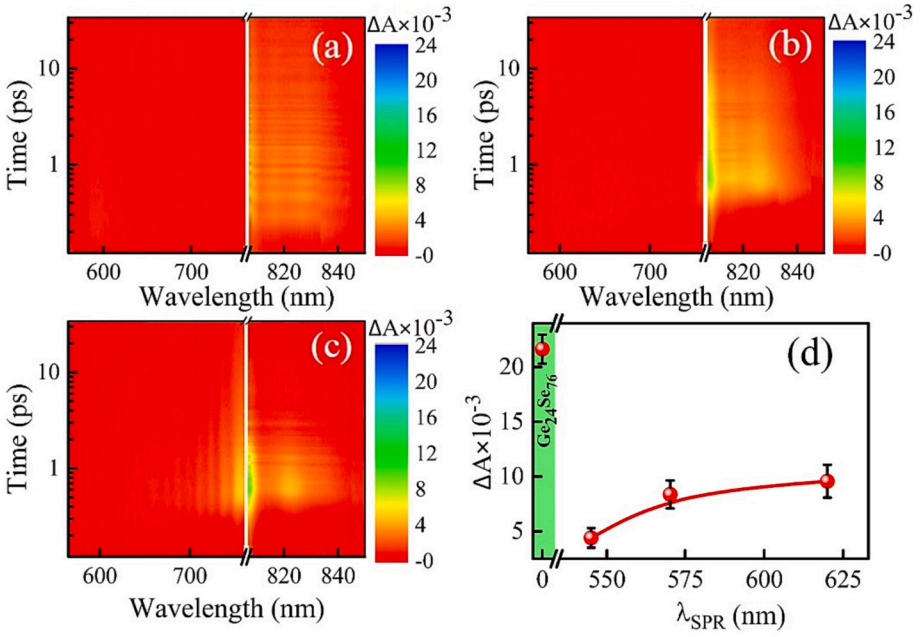

Fig. 5. Contour plots of TA spectra for (a) HS-1 (b) HS-2 and (c) HS-3 (d) Comparison of change in absorption corresponding to excitonic maxima (λ = 807 nm) for different HS. Surface plasmon resonance (λ_{SPR}) =0 corresponds to pristine $Ge_{24}Se_{76}$.

4. Conclusions

In summary, we demonstrate the third-order nonlinear optical response in charge coupled AuNP/$Ge_{24}Se_{76}$ heterostructures within the strong coupling regime enabled by the charge transfer. We have observed a sign reversal of ultrafast third-order nonlinear absorption and refraction in heterostructures compared to pristine $Ge_{24}Se_{76}$. For instance, in sharp contrast to the weak two-photon absorption (TPA) and self-focusing (positive nonlinearity) of $Ge_{24}Se_{76}$ the strongly coupled heterostructure shows saturable absorption (SA) and self-defocusing (negative nonlinearity). Moreover, the enhanced blue shifted Raman signal and narrow spectral width of the ultrafast transient absorption and quenching of localized surface plasmon absorption in the heterostructure supports the thesis of the charge transfer between pristine $Ge_{24}Se_{76}$ and AuNP. All these studies clearly show that the coupling between amorphous materials and metal nanoparticles can generate a wide range of exciting opportunities for novel optical functionalities not exhibited by the individual components. These developments hold tremendous potential for developing new device technologies, such as all-optical data processing, data storage, passive mode-lock saturable absorber and semiconductor devices.

Declaration of Competing Interest

The authors declare that they have no known competing financial interests or personal relationships that could have appeared to influence the work reported in this paper.

Data availability

No data was used for the research described in the article.

Acknowledgements

The authors thank the Science and Engineering Research Board (CRG/2019/002808); the Department of Science and Technology, Ministry of Science and Technology, India (DST-FIST project (PSI-195/2014) for financial support. Istvan Csarnovics acknowledges the János Bolyai Research Scholarship from the Hungarian Academy of Sciences (BO/348/20). The New National Excellence Program's ÚNKP-22-3-II-DE-53 and ÚNKP-22-5-DE-407 also provided support from the National Research, Development, and Innovation Fund. The US National Science Foundation is acknowledged for supporting (DMR-2123131) this international collaboration that was established through International Materials Institute for New Functionality in Glass (DMR-0844014).

References

[1] K. Tvrdy, P.A. Frantsuzov, P.V. Kamat, Photoinduced electron transfer from semiconductor quantum dots to metal oxide nanoparticles, Proc. Natl. Acad. Sci. U. S. A. 108 (2011) 29–34.
[2] P. Vasa, R. Pomraenke, S. Schwieger, Y.I. Mazur, V. Kunets, P. Srinivasan, E. Johnson, J.E. Kihm, D.S. Kim, E. Runge, G. Salamo, C. Lienau, Coherent exciton-surface-plasmon-polariton interaction in hybrid metal-semiconductor nanostructures, Phys. Rev. Lett. 101 (2008), 116801.
[3] G. Zengin, M. Wersäll, S. Nilsson, T.J. Antosiewicz, M. Käll, T. Shegai, Realizing strong light-matter interactions between single-nanoparticle plasmons and molecular excitons at ambient conditions, Phys. Rev. Lett. 114 (2015), 157401.
[4] A. Salah, A.S. Mansour, M.B. Mohamed, S.H. Elnaby, Nonlinear absorption and optical limiting of Ag-CdSe nano-hybrids of different growth times, Optik 181 (2019) 278–286.
[5] R.K. Yadav, J. Aneesh, R. Sharma, P. Abhiramnath, T.K. Maji, G.J. Omar, A. K. Mishra, D. Karmakar, K.V. Adarsh, Designing hybrids of graphene oxide and gold nanoparticles for nonlinear optical response, Phys. Rev. Appl. 9 (2018), 044043.
[6] M.H.M. Ahmed, A.A. Latiff, H. Arof, S.W. Harun, Mode-locking pulse generation with MoS_2–PVA saturable absorber in both anomalous and ultra-long normal dispersion regimes, Appl. Opt. 55 (2016) 4247–4252.
[7] V. Pusino, M.J. Strain, M. Sorel, Passive mode-locking in semiconductor lasers with saturable absorbers bandgap shifted through quantum well intermixing, Photon. Res. 2 (2014) 186–189.
[8] R. Sharma, J. Aneesh, R.K. Yadav, S. Sanda, A.R. Barik, A.K. Mishra, T.K. Maji, D. Karmakar, K.V. Adarsh, Strong interlayer coupling mediated giant two-photon absorption in $MoSe_2$/graphene oxide heterostructure: quenching of exciton bands, Phys. Rev. B 93 (2016), 155433.
[9] Z.-B. Liu, X. Zhao, X.-L. Zhang, X.-Q. Yan, Y.-P. Wu, Y.-S. Chen, J.-G. Tian, Ultrafast dynamics and nonlinear optical responses from Sp^{2-} and Sp^{3-} hybridized domains in graphene oxide, J. Phys. Chem. Lett. 2 (2011) 1972.
[10] X. Sun, B. Zhang, Y. Li, X. Luo, G. Li, Y. Chen, C. Zhang, J. He, Tunable ultrafast nonlinear optical properties of graphene/MoS2 van der Waals heterostructures and their application in solid-state bulk lasers, ACS Nano 12 (2018) 11376–11385.
[11] S.K. Dutta, S.K. Mehetor, N. Pradhan, Metal semiconductor Heterostructures for photocatalytic conversion of light energy, J. Phys. Chem. Lett. 6 (2015) 936–944.
[12] Y.M. Di, J.Y. Liu, M.H. Li, S.Q. Zhang, M.H. You, M.J. Lin, Donor–acceptor hybrid heterostructures: an emerging class of photoactive materials with inorganic and organic semiconductive components, Small 18 (2022) 2201159.
[13] S. Huang, D. Ma, Z.J. Hu, Q. He, J. Zai, D. Chen, H. Sun, Z. Chen, Q. Qiao, M. Wu, X. Qian, Synergistically enhanced electrochemical performance of Ni3S4–PtX (X = Fe, Ni) Heteronanorods as heterogeneous catalysts in dye-sensitized solar cells, ACS Appl. Mater. Interfaces 9 (2017) 27607–27617.
[14] R. Rosati, I. Paradisanos, L. Huang, et al., Interface engineering of charge-transfer excitons in 2D lateral heterostructures, Nat. Commun. 14 (2023) 2438.
[15] Z. Xue, H. Yang, J. Gao, J. Li, Y. Chen, Z. Jia, Y. Li, H. Liu, W. Yang, Y. Li, D. Li, ACS Applied Materials & Interfaces 8, 2016, pp. 21563–21569.
[16] R.K. Yadav, J. Aneesh, R. Sharma, S.K. Bera, T.K. Maji, D. Karmakar, K.P. Loh, K. V. Adarsh, Ultrafast direct charge transfers mediated modification of third order nonlinear optical response in Sb_2Se_3–au core shell nanorods, Appl. Phys. Lett. 117 (2020), 032104.
[17] V. Kumar, D. Mandal, K.A. Sree Raj, B. Chakraborty, A. Agarwal, C.S. Rout, K. V. Adarsh, Single-wall-carbon-nanotube–VSe_2 nanohybrid for ultrafast visible-to-near-infrared third-order nonlinear optical limiters, Phys. Rev. Appl. 19 (2023), 044081.
[18] F. Nan, S. Liang, X.L. Liu, X.N. Peng, M. Li, Z.J. Yang, L. Zhou, Z.H. Hao, Q. Q. Wang, Sign-reversed and magnitudeenhanced nonlinear absorption of au−CdS core−shell heteronanorods, Appl. Phys. Lett. 102 (2013), 163112.
[19] M. Fu, K. Wang, H. Long, G. Yang, P. Lu, F. Hetsch, A.S. Susha, A.L. Rogach, Resonantly enhanced optical nonlinearity in hybrid semiconductor quantum dot−metal nanoparticle structures, Appl. Phys. Lett. 100 (2012), 063117.
[20] V.I. Klimov, D.W. McBranch, Femtosecond high-sensitivity, chirp-free transient absorption spectroscopy using kilohertz lasers, Opt. Lett. 23 (1998) 277–279.
[21] R. Sharma, P. Khan, J. Aneesh, K.S. Sangunni, I. Csarnovics, S. Kokenyesi, H. Jain, K.V. Adarsh, Strong exciton-localized plasmon coupling in a-$Ge_{24}Se_{76}$/AuNP heterostructure, APL Mater. 4 (2016), 106105.
[22] I. Csarnovics, M. Veres, P. Nemec, S. Molnár, S. Kökényesi, Surface plasmon enhanced light-induced changes in GeSe amorphous chalcogenide – gold nanostructures, J. Non-Cryst. Solids X 6 (2020), 100045.
[23] J. Burunkova, I. Csarnovics, I. Denisyuk, L. Daróczi, S. Kökényesi, Enhancement of laser recording in gold/amorphous chalcogenide and gold/acrylate nanocomposite layers, J. Non-Cryst. Solids 402 (2014) 200–203.
[24] M.J. Rost, D.A. Quist, J.W.M. Frenken, Grains, growth, and grooving, Phys. Rev. Lett. 91 (2003), 026101.
[25] Y. Ben-Shahar, F. Scotognella, I. Kriegel, L. Moretti, G. Cerullo, E. Rabani, U. Banin, Optimal metal domain size for photocatalysis with hybrid semiconductor-metal nanorods, Nat. Commun. 7 (2016) 1–7.
[26] R.W. Schurko, R.E. Wasylishen, J.H. Nelson, Effect of cobalt-59 self-decoupling on the solid-state 31P CP/MAS NMR spectra of cobaloximes, J. Phys. Chem. 100 (1996) 8053–8056.
[27] K. Jackson, A. Briley, S. Grossman, D.V. Porezag, M.R. Pederson, Raman-active modes of a − GeSe2 and a − GeS2 : a first-principles study, Phys. Rev. B 60 (1999) 14985.
[28] M.T. Shatnawi, C.L. Farrow, P. Chen, P. Boolchand, A. Sartbaeva, M. Thorpe, S.J. L. Billinge, Search for a structural response to the intermediate phase in GexSe1 − x glasses, Phys. Rev. B 77 (2008), 094134.
[29] M. Olivier, J.C. Tchahame, P. Němec, M. Chauvet, V. Besse, C. Cassagne, G. Boudebs, G. Renversez, R. Boidin, E. Baudet, V. Nazabal, Structure, nonlinear properties, and photosensitivity of ($GeSe_2$)100-x(Sb_2Se_3)x glasses, Opt. Mat. Exp. 4 (2014) 525–540.
[30] P. Khan, H. Jain, K.V. Adarsh, Role of Ge:As ratio in controlling the light-induced response of a-$GexAs_{35-x}Se_{65}$ thin films, Sci. Rep. 4 (2014) 4029.
[31] P.A. González, P. Albella, M. Schnell, J. Chen, F. Huth, A. García-Etxarri, F. Casanova, F. Golmar, L. Arzubiaga, L.E. Hueso, J. Aizpurua, R. Hillenbrand, Resolving the electromagnetic mechanism of surface-enhanced light scattering at single hot spots, Nat. Commun. 3 (2012) 1–12.
[32] E.C. Le Ru, E. Blackie, M. Meyer, P.G. Etchegoin, Surface enhanced Raman scattering enhancement factors: a comprehensive study, J. Phys. Chem. C 111 (2007) 13794.
[33] K. Shimakawa, A. Kolobov, S.R. Elliott, Photoinduced effects and metastability in amorphous semiconductors and insulators, Adv. Phys. 44 (1995) 475.
[34] Xiaolei Zhang, Yu Zhi, Wei Ji, Huimin Sui, Qian Cong, Xu Wang, Bing Zhao, Charge-transfer effect on surface-enhanced Raman scattering (SERS) in an ordered Ag NPs/4-Mercaptobenzoic acid/TiO2 system, J. Phys. Chem. C 119 (2015) 22439–22444.
[35] B.S. Kalanoor, L. Gouda, R. Gottesman, S. Tirosh, E. Haltzi, A. Zaban, Y.R. Tischler, Third-order optical nonlinearities in organometallic methylammonium lead iodide perovskite thin films, ACS Photonics 3 (2016) 361.

[36] S. Link, C. Burda, M. Mohamed, B. Nikoobakht, M. El-Sayed, Femtosecond transient-absorption dynamics of colloidal gold nanorods: shape independence of the electron-phonon relaxation time, Phys. Rev. B 61 (2000) 6086.
[37] A.R. Barik, M. Bapna, D.A. Drabold, K.V. Adarsh, Ultrafast light induced unusually broad transient absorption in the sub-bandgap region of $GeSe_2$ thin film, Sci. Rep. 4 (2014) 1–5.
[38] R.A. Street, Recombination in amorphous semiconductors, Phys. Rev. B 17 (1978) 3984.
[39] P. Pradhan, P. Khan, J.R. Aswin, K.V. Adarsh, R. Naik, N. Das, A.K. Panda, Quantification of nonlinear absorption in ternary as-Sb-se chalcogenide glasses, J. Appl. Phys. 125 (2019), 015105.